THE USE OF CHIRPED FIBRE BRAGG GRATING SENSORS TO MONITOR DISBOND GROWTH

GT Reed[1], SL Ogin[2], AD Crocombe[2], AM Thorne[2], J Palaniappan[2], TF Capell[2], SC Tjin[3] and L Mohanty[3]

[1] Advanced Technology Institute, Department of Electronic Engineering, University of Surrey, GU2 7XH, UK
[2] Faculty of Engineering & Physical Sciences, University of Surrey, Guildford, Surrey, GU2 7XH, UK
[3]School of Electrical and Electronic Engineering, Nanyang Technological University, Nanyang Avenue, Singapore 639798, Singapore

Introduction

Composite-composite or composite-metal bonded joints, are used in various industries and applications. The difficulty with any bonded construction with regard to structural integrity monitoring is, of course, that the bonded structure cannot be disassembled easily. Various NDE (non-destructive evaluation) techniques have been suggested to monitor bonded joints based on ultrasonic, acoustic, thermal and backface strain measurements [e.g. 1-3]. Among NDE optical techniques suggested, the use of uniform fibre Bragg grating (FBG) sensors has been the most widely favoured, with a number of demonstrations available in the literature for monitoring bonded joints, repairs and structures [e.g. 4-6]. In addition, chirped fibre Bragg grating (CFBG) sensors have been investigated more recently for damage monitoring in composite materials, bonded joints and sandwich structures (e.g. [7-11]).

Experimental

Sample Preparation

In this work both composite-composite and composite-metal joints are discussed, with a view to monitoring initiation and growth of disbonds. Both were configured as single lap joints.

Transparent glass fibre reinforced plastic (GFRP) adherends with the lay-up $(0_2/90/0_6)_s$ have been used for the composite material adherend in both types of bonded joints so that the development of disbonding damage between the composite/composite or the composite/aluminium adherends can be photographed for direct comparison with the sensor measurements. Single mode optical fibres, 125μm in diameter, containing the CFBG sensors were embedded within the composite adherends, with the optical fibres located at the first 0/90 interface closest to the bondline. The thickness of each ply of the GFRP adherends was 0.25 mm, giving an overall thickness of 4.5 mm. In the case of the composite/aluminium joints, the alloy used for the second adherend in the single lap joint (SLJ) was a 1000 series alloy with a thickness of 1.94 mm. For the composite/composite lap joints, a range of sensor lengths have been used (15, 30, 45, and 60mm), whereas for the composite/metal joints, lengths of 60mm have been used, although all sensors had a spectral width of 20nm at Full Width, Half Maximum (FWHM).

Setup and Procedure

The optical arrangement consisted of a broadband light source connected to a 3 dB coupler which both carries light to the optical fibre embedded in the GFRP adherend and takes reflected light from the CFBG sensor back to an optical spectrum analyser. The SLJs were loaded in fatigue using a computer-controlled servo-hydraulic fatigue machine (Instron 1341) under load control. The SLJs were tested with a peak cyclic load of 5.5 kN and a minimum load of 0.55 kN, using a sinusoidal waveform and a frequency of 5 Hz. The cyclic loading was interrupted at intervals (typically after 1000 to 3000 cycles) when the SLJ was unloaded in order (a) to photograph the development of the progression of the disbond, and (b) to record the reflected spectrum, which required a small quasi-static load for the composite/composite joints.

Results and Discussion

1.0 Composite/Composite Lap joints

Disbond monitoring at the low-wavelength end

In previous work [10] using a CFBG sensor with a length of 45 mm, it was shown that a disbond initiating adjacent to the low-wavelength end of the sensor could be detected. Figure 1 shows the reflected spectra before and after the initiation of a disbond for a CFBG sensor length of 15 mm. It can be seen that after the disbond initiates, the low-wavelength end of the reflected spectrum moves to lower wavelengths. When the disbond initiates, a short length of adherend adjacent to the disbond is unloaded and hence relaxes, causing the sensor spacing to reduce locally, so that the low wavelength end of the spectrum moves to lower wavelengths. The dip in both spectra at about 1549 nm corresponds to the position of the wire spacer used to ensure a uniform adhesive bondline.

Figure 2 shows the entire 60 mm overlap length of the transparent GFRP-GFRP bonded joint containing the 15 mm CFBG sensor after 14,000, 15,000, 17,000 and 19,000 cycles, with the arrows indicating the position of the sensor in relation to the growing disbond front. The progression of the disbond front is indicated in the reflection spectrum by a distinct perturbation in the spectrum which moves to higher wavelengths as the disbond front grows.

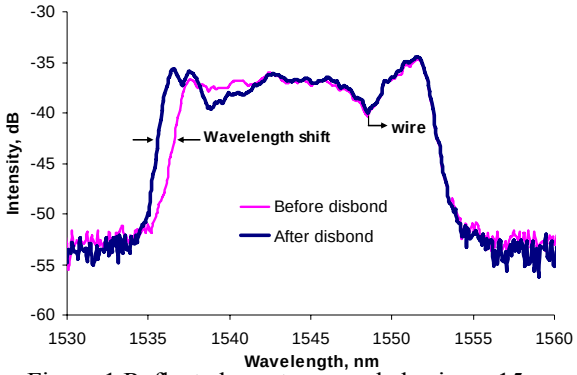

Figure 1 Reflected spectra recorded using a 15 mm CFBG sensor under a small tensile load, before and after disbonding. The shift in the low-wavelength end of the spectrum to lower wavelengths indicates disbond initiation.

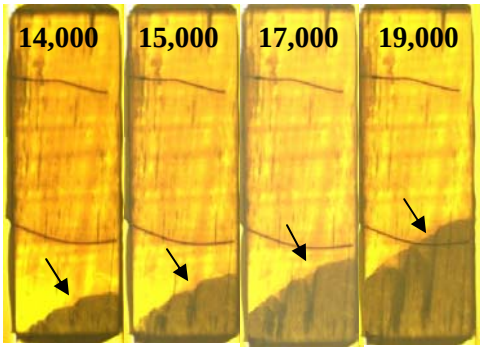

Figure 2. Growth of a disbond in a transparent GFRP-GFRP bonded joint; the arrows indicate the CFBG sensor position relative to the disbond front position.

Disbonding at the high-wavelength end

A disbond can initiate at either end of a single lap-joint and this section shows that a disbond initiating at the high wavelength end can also be monitored. Figure 3 shows the reflected spectra for a CFBG sensor which extends the full length of a 60 mm bonded joint, both before and after disbond initiation. Figure 3 compares a reflected spectrum before and after 25,000 fatigue cycles, by which point a disbond had initiated adjacent to the high-wavelength end of the sensor. The fatigue parameters for this experiment were the same as described earlier, and again the spectra were recorded under a load of 5 kN. In this case, there is a shift in the high wavelength end of the CFBG reflected spectrum to higher wavelengths as a consequence of disbond initiation. For this configuration, when the SLJ disbonds at the high wavelength end, the disbond enhances the load locally in the adherend which contains the embedded sensor. The adherend experiences an enhanced strain, which leads locally to an increased period of the gratings of the CFBG sensor, and the reflected spectrum here shifts to higher wavelengths.

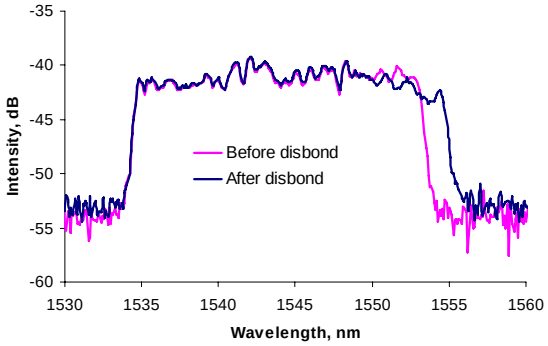

Figure 3. Comparison of reflected spectra for a 60 mm CFBG sensor before/after disbond initiation. The disbond occurs adjacent to the high-wavelength end of the sensor.

2.0 Composite/Metal Lap Joints

Internal strains after fabrication of the single lap joint

The embedded CFBG sensor enables the strain in the GFRP adherend to be measured after manufacture of the single lap joint. The adhesive bond of the SLJ is formed at elevated temperature so that when the GFRP and aluminium adherends cool to room temperature, the differences in the coefficients of thermal expansion (CTE) produces residual thermal strains in each adherend. Parallel to the length of the SLJ, the aluminium adherend experiences a tensile strain (relative to its initial length at room temperature) and the GFRP experiences a compressive strain, since the coefficient of thermal expansion (CTE) of the aluminium is much greater than that of the GFRP. The strain experienced by the CFBG as a consequence of the thermal mismatch between the GFRP and the aluminium adherends is predicted to be about 1140με [9]. This corresponds to a predicted shift of the CFBG reflected spectrum of 1.14 nm towards lower wavelengths, assuming the typical strain sensitivity for CFBG gratings of this type to be approximately 1 x 10^{-3} nm/με [12]. Figure 4 shows the experimentally measured shift is about 0.81 nm. The difference is probably mainly due to end effects in the

SLJ, whereas the strain in the SLJ has been assumed to be uniform along its entire bonded length. Additionally, some of the thermal strain in the adherends may have been relaxed as a result of shear relaxation within the adhesive.

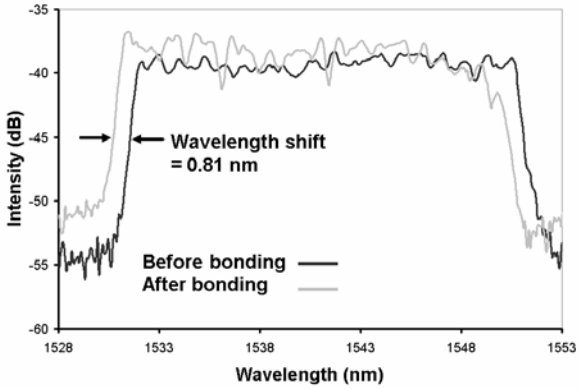

Figure 4 Wavelength shift in the GFRP after bonding the GRFP and aluminium adherends

Detection of disbond initiation

The detection of disbond initiation is illustrated by the spectra of figure 5, which compares the reflected spectra before and after 3000 fatigue cycles, by which point a disbond has initiated. The shift in the low-wavelength end of the reflected spectra to higher wavelengths can be explained as follows. The manufacture of the bonded joint generates compressive thermal strains in the GFRP adherend. When the SLJ disbond initiates, the thermal strain is relaxed locally as a result of the disbond and hence that part of the CFBG sensor embedded within the disbonded region of the GFRP adherend is allowed to return to its unstrained state. Consequently, the grating periods at the low-wavelength end of the sensor, which is near the adherend end, increase in length and the low-wavelength end of the reflected spectrum is shifted to higher wavelengths. The disbond front is not uniform across the width of the SLJ (as will be seen in the next section), so the relaxation due to disbond initiation is not yet complete.

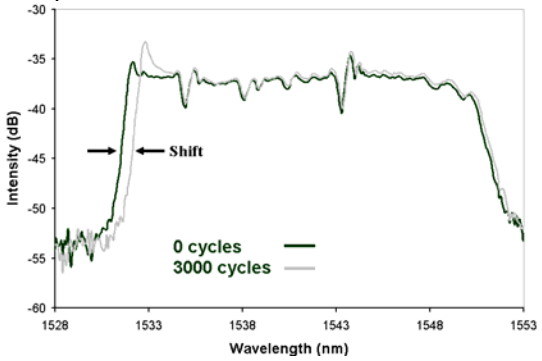

Figure 5. Shift of the low-wavelength end of the CFBG reflected spectrum to higher wavelengths after disbond initiation

The spectra shown in figure 5 also show two distinct perturbations at about 1535 nm and 1544 nm. These perturbations correspond to the physical positions of the two wires that were used to produce a uniform adhesive thickness during the manufacture of the bonded joint. The bond was formed under light pressure and, although the optical fibre is embedded within the GFRP adherend (at a distance of about 0.5 mm from the adherend surface, which is the location of the first 0/90 interface), the CFBG sensor is sufficiently sensitive to local strain changes to detect the strain field caused by the two wires, thus producing perturbations in the spectra at the wire locations.

Monitoring of disbond growth

Photographs showing an example of the progression of a disbond front as a result of fatigue cycling are shown in figure 6, where arrows indicate the position of the disbond front after increasing numbers of fatigue cycles. After 7000 cycles, the disbond has grown to a length of about 9 mm, progressing to a length of about 22 mm after 11,000 cycles.

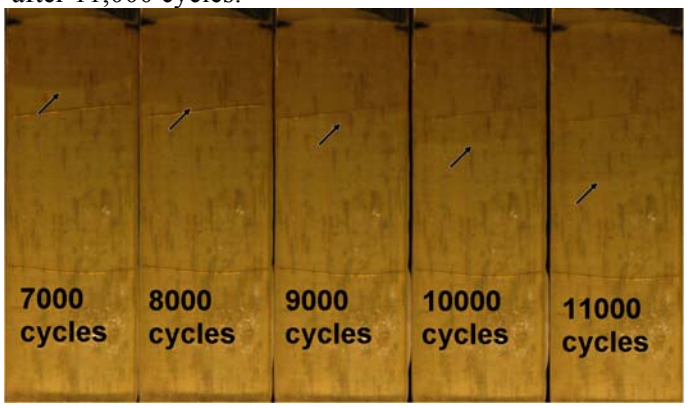

Figure 6. Photographs of disbond growth from the end of the GFRP adherend (which is also the low wavelength end of the CFBG)

As the disbond front advances, a peak in the CFBG sensor reflected spectrum caused by the relaxation of the compressive thermal strain in the GFRP adherend moves to higher wavelengths. Figure 7 shows examples of the reflected spectrum for 7000, 8000 and 10,000 cycles, with the peak in the reflected spectrum indicated by an arrow. The peak in the spectrum is caused by relaxation of the grating period in the disbonded region, so that the gratings in this region now correspond in size to the grating periods just ahead of the disbond front, where the gratings have not yet been relaxed. The intensity of the reflected spectrum of a chirped grating is related to the local density of grating period; hence, an increase in the density of the grating period leads to an increase in

reflected intensity, and consequently a peak in the spectrum. As the disbond front progresses, so the peak in the spectrum moves to higher wavelengths.

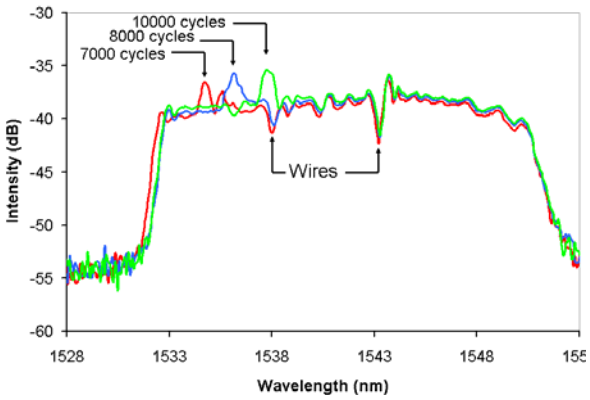

Figure 7. Detection of disbond growth with fatigue cycling for a disbond initiating adjacent to the low wavelength end of a CFBG sensor

It can be shown [9], that the movement of the peak in the reflected spectrum accurately tracks the increase in the disbond length. Interestingly, the position of the disbond front can still be detected using the CFBG technique if the disbond begins at the high wavelength end of the CFBG sensor i.e. at the termination of the GFRP adherend. In this case, the disbond again relaxes the grating period within the disbonded GFRP adherend, so that the grating periods increase in the disbonded region. The consequence now is that particular grating periods at the disbond front are "lost" due to this relaxation, causing a reduction in intensity and a dip in the reflected spectrum; this dip moves to lower reflected wavelengths as the disbond grows.

Conclusions

This paper has shown that a chirped fibre Bragg grating sensor can be used to monitor disbonding at either end of an adhesively bonded single-lap joint, with the sensor embedded within one adherend and with the low-wavelength end of the sensor at the cut end of the adherend. Disbond initiation adjacent to either the low-wavelength or high-wavelength end of the sensor is indicated by a shift in the low wavelength end of the spectrum to lower wavelengths (for disbonding adjacent to the low-wavelength end) or a shift in the high wavelength end of the spectrum to higher wavelengths (for disbonding adjacent to the high-wavelength end). Disbond propagation is shown by the movement of a perturbation in the reflected spectrum which corresponds to the progression of the disbond front: The detailed shape of the perturbation depends upon the CFBG chirp rate, but in all cases a combination of finite-element modelling and commercial FBG software enables the position of the disbond front to be related to the perturbation in the reflected spectrum. In general, the position of the disbond front can be located with a precision of about 2 mm.

Relaxation of thermal residual strains (generated within the joint during manufacture) also enables disbond initiation and disbond propagation to be detected when composite /metal joint is unloaded. For disbonds initiating adjacent to the end of the aluminium adherend, a shift in the low-wavelength end of the reflected spectrum to higher wavelengths is an indication of disbond *initiation*.

References

1. Cawley P. Proc. IEEE 1992: 767-772.
2. Lowe MJS , Challis RE, Chan CW. J. Acous. Soc. Am. 2000; 107(3):1333-1345.
3. Crocombe AD, Ong CY, Chan CM, Wahab MA, Ashcroft IA. J. Adhesion 2002; 78(9): 745-778.
4. Kuang KSC, Cantwell WJ. Appl. Mech. Rev. 2003; 56: 493-513.
5. Takeda S, Aoki Y, Ishikawa, Takeda N, Kikukawa. Compos. Struct. 2007; 79:133-139.
6. Ussorio M, Wang H, Ogin SL, Thorne AM, Reed GT, Tjin SC, Suresh R. Construct. Build. Mater. 2006;20(1) :111-118
7. Palaniappan J, Wang H, Ogin SL, Thorne AM, Reed GT, Tjin SC, McCartney LN. Meas. Sci. Technol. 2006; 17(6):1609-1614.
8. Takeda S, Okabe Y, Takeda N. Proc. SPIE 2003; 5050: 171-178.
9. Capell T F, Palaniappan J, Ogin S L, Crocombe A D, Reed G T, Thorne A M, Mohanty L and Tjin S C. *J. Opt. A: Pure Appl. Opt.* ***9*** (2007) S40-S44.
10. Palaniappan J, Wang H, Ogin SL, Thorne AM, Reed GT, Crocombe AD, Tjin SC. Adv. Comp. Letters 2005; 14(6):185-192.
11. Palaniappan J, Wang H, Ogin S L, Thorne A M, Reed G T, Crocombe A D, Tjin SC. Compos. Sci. Technol. 2007; 67(13), 2847-2853.
12. Palaniappan J, unpublished.